© 2017. Published by The Company of Biologists Ltd | Development (2017) 144, 441-451 doi:10.1242/dev.147074

RESEARCH ARTICLE

Sirt1 regulates acrosome biogenesis by modulating autophagic flux during spermiogenesis in mice

Chao Liu[1,*], Zhenhua Song[1,2,3,*], Lina Wang[1,2,*], Haiyan Yu[1,2], Weixiao Liu[1], Yongliang Shang[1,2], Zhiliang Xu[1,2], Haichao Zhao[1,2], Fengyi Gao[1], Jiamin Wen[1,2], Linan Zhao[1], Yaoting Gui[4], Jianwei Jiao[1], Fei Gao[1] and Wei Li[1,‡]

ABSTRACT

Sirt1 is a member of the sirtuin family of proteins and has important roles in numerous biological processes. *Sirt1*$^{-/-}$ mice display an increased frequency of abnormal spermatozoa, but the mechanism of Sirt1 in spermiogenesis remains largely unknown. Here, we report that Sirt1 might be directly involved in spermiogenesis in germ cells but not in steroidogenic cells. Germ cell-specific *Sirt1* knockout mice were almost completely infertile; the early mitotic and meiotic progression of germ cells in spermatogenesis were not obviously affected after Sirt1 depletion, but subsequent spermiogenesis was disrupted by a defect in acrosome biogenesis, which resulted in a phenotype similar to that observed in human globozoospermia. In addition, LC3 and Atg7 deacetylation was disrupted in spermatids after knocking out *Sirt1*, which affected the redistribution of LC3 from the nucleus to the cytoplasm and the activation of autophagy. Furthermore, Sirt1 depletion resulted in the failure of LC3 to be recruited to Golgi apparatus-derived vesicles and in the failure of GOPC and PICK1 to be recruited to nucleus-associated acrosomal vesicles. Taken together, these findings reveal that Sirt1 has a novel physiological function in acrosome biogenesis.

KEY WORDS: Sirt1, Map1lc3, Acrosome biogenesis, Globozoospermia, Deacetylation, Autophagy, Mouse

INTRODUCTION

Infertility is estimated to affect up to 15% of couples of reproductive age (Boivin et al., 2007). Globozoospermia is a rare but severe disorder causing male infertility that is characterized by round-headed spermatozoa and an absent or highly abnormal acrosomal compartment (Dam et al., 2007; Kullander and Rausing, 1975; Lalonde et al., 1988; Singh, 1992). The acrosome is a cap-shaped, Golgi-derived organelle that is located over the anterior part of the sperm nucleus. The morphogenic changes of acrosome biogenesis during spermiogenesis have been well documented; numerous proacrosomal granules derived from *trans*-Golgi stacks accumulate in the concave region near the *trans*-Golgi stacks and fuse with each other while they bind to the acroplaxome (a cytoskeletal structure attached to the nuclear envelope) (Kierszenbaum et al., 2003) and then generate the acrosomal vesicle. Additional vesicle fusion increases acrosome size and, together with nucleus reformation, the acrosome adopts its characteristic shape (Abou-Haila and Tulsiani, 2000). Genetically modified mouse models have been helpful in understanding the molecular mechanisms underlying acrosome biogenesis, and several genes have been identified as associated with globozoospermia, including *Csnk2a2* (Xu et al., 1999), *Hrb* (*Agfg1*) (Kang-Decker et al., 2001), *Gopc* (Yao et al., 2002), *Gba2* (Yildiz et al., 2006), *Zpbp1* (Lin et al., 2007), *Pick1* (Xiao et al., 2009), *Hsp90b1* (Audouard and Christians, 2011), *Vps54* (Paiardi et al., 2011), *Spaca1* (Fujihara et al., 2012) and *Dpy19l2* (Pierre et al., 2012). Recently, we found that Atg7 is involved in the transportation/fusion of Golgi-derived proacrosomal vesicles to form the nucleus-associated acrosome (Wang et al., 2014). However, much of the aetiology of globozoospermia remains unknown, and the mechanism underlying acrosome biogenesis remains elusive.

Sirt1 is a member of the mammalian sirtuin gene family and is the closest relative of yeast Sir2 in mammalian cells (Brachmann et al., 1995; Smith et al., 2000). By deacetylating a number of substrates, Sirt1 regulates numerous important physiological processes, including glucose metabolism, cell survival, mitochondrial respiration and histone modification. Sirt1 is not essential to survival in mice; however, *Sirt1*$^{-/-}$ male mice are infertile (McBurney et al., 2003). It has been proposed that Sirt1 might regulate spermatogenesis at postnatal stages by controlling hypothalamus-pituitary gonadotropin (HPG) signalling (Kolthur-Seetharam et al., 2009). A detailed analysis of the functions of Sirt1 in the germ line of *Sirt1*$^{-/-}$ mice (Coussens et al., 2008) and meiotic-specific *Sirt1* knockout mice revealed that Sirt1 might be involved in the differentiation of spermatogenic stem cells and the transition from histone to protamine (Bell et al., 2014). In addition, the researchers found an increased proportion of abnormal spermatozoa in the Sirt1-deficient mice; however, the mechanism by which Sirt1 deficiency in germ cells leads to malformed spermatozoa and the identity of its specific substrate during spermiogenesis remain largely unknown.

To study the role of Sirt1 during spermiogenesis, we generated steroidogenic cell-specific and germ cell-specific *Sirt1* knockout mouse lines by crossing *Sirt1*$^{F/F}$ mice with *SF1-Cre* and *Tnap-Cre* mice, respectively (Bingham et al., 2006; Lomeli et al., 2000). We found that the malformed spermatozoa in Sirt1-deficient mice were primarily caused by Sirt1 deficiency in germ cells rather than in the steroidogenic cells. Further investigation revealed that Sirt1 depletion in germ cells led to the accumulation of acetylated LC3 in the spermatid nucleus, and this affected the recruitment of several acrosome biogenesis-related proteins to nucleus-associated acrosomal vesicles. Therefore, our study reveals a novel function for Sirt1 during acrosome biogenesis.

[1]State Key Laboratory of Stem cell and Reproductive Biology, Institute of Zoology, Chinese Academy of Sciences, Beijing 100101, People's Republic of China. [2]University of Chinese Academy of Sciences, Beijing 100049, People's Republic of China. [3]Department of Pharmacology, Qingdao University School of Pharmacy, Qingdao 266021, People's Republic of China. [4]Guangdong Key Laboratory of Male Reproductive Medicine and Genetics, Peking University Shenzhen Hospital, Shenzhen 518035, People's Republic of China.
*These authors contributed equally to this work

‡Author for correspondence (leways@ioz.ac.cn)

W.L., 0000-0002-6235-0749

Received 16 November 2016; Accepted 4 December 2016

Development (2017) 144, 441-451 doi:10.1242/dev.147074

RESULTS

Spermatogenesis is not disrupted in steroidogenic cell-specific *Sirt1* knockout mice

To test whether Sirt1 deficiency in steroidogenic cells disrupts spermatogenesis in testis, we generated a steroidogenic cell-specific *Sirt1* knockout mouse line by crossing $Sirt1^{F/F}$ mice with *SF1-Cre* mouse strains. *SF1-Cre* [in which Cre is driven by steroidogenic factor 1 (*SF1*; also known as *Nr5a1*)] is predominately expressed in pituitary, adrenal gland and Leydig cells in testis (Bingham et al., 2006), and its expression resulted in steroidogenic cell-specific *Sirt1* knockout in $Sirt1^{F/F}$*; SF1-Cre* mice. Western blotting showed that the protein level of Sirt1 was dramatically reduced in the Leydig cells of $Sirt1^{F/F}$*; SF1-Cre* compared with $Sirt1^{F/F}$ mice (Fig. S1A).

As Sirt1 has been reported to regulate testosterone synthesis by controlling HPG signalling (Kolthur-Seetharam et al., 2009), we assessed mating efficiency and testosterone concentrations in $Sirt1^{F/F}$ and $Sirt1^{F/F}$*; SF1-Cre* male mice. Both were decreased in $Sirt1^{F/F}$*; SF1-Cre* male mice compared with control groups (Fig. S1B,C). However, no significant difference in testis size (Fig. S1D) was observed between $Sirt1^{F/F}$ and $Sirt1^{F/F}$*; SF1-Cre* mice. Histological analysis of testis and epididymis also showed no obvious defect compared with control mice (Fig. S1E,F). When spermatozoa released from the cauda epididymis were assessed, no abnormal spermatozoa were found in either the $Sirt1^{F/F}$ or $Sirt1^{F/F}$*; SF1-Cre* mice (Fig. S1G). Furthermore, the average epididymal sperm count of $Sirt1^{F/F}$*; SF1-Cre* mice was similar to that of $Sirt1^{F/F}$ mice (Fig. S1H), and this was accompanied by high sperm motility (Fig. S1I).

These results suggest that the disruption of Sirt1 in steroidogenic cells might affect sexual behaviour, but not spermatogenesis, indicating that the malformed spermatozoa defect of $Sirt1^{-/-}$ mice might not be caused by Sirt1 deficiency in steroidogenic cells.

Germ cell-specific *Sirt1* knockout causes infertility in male mice

To address the function of Sirt1 during spermatogenesis, *Sirt1* was specifically knocked out in germ cells by crossing $Sirt1^{F/F}$ mice with *Tnap-Cre* mouse strains. *Tnap-Cre* [in which Cre is driven by tissue non-specific alkaline phosphatase (*Tnap*; also known as *Alpl*)] is specifically expressed in primordial germ cells (Lomeli et al., 2000), which resulted in germ cell-specific *Sirt1* knockout in $Sirt1^{F/F}$*; Tnap-Cre* mice. The Sirt1 protein level was dramatically reduced in the testis of $Sirt1^{F/F}$*; Tnap-Cre* compared with $Sirt1^{F/F}$ mice (Fig. 1A), confirming Sirt1 deficiency in these germ cells.

To test male fertility after germ cell-specific *Sirt1* knockout, a breeding assay was conducted by mating $Sirt1^{F/F}$ or $Sirt1^{F/F}$*; Tnap-Cre* male mice with $Sirt1^{F/F}$ females over a 2 month period. As shown in Fig. 1B, $Sirt1^{F/F}$*; Tnap-Cre* male mice were severely subfertile; only 19.83% of the females mating with $Sirt1^{F/F}$*; Tnap-Cre* male mice became pregnant compared with 82.67% of those mating with $Sirt1^{F/F}$ males. Both the size and weight of the testes of $Sirt1^{F/F}$*; Tnap-Cre* mice were reduced compared with those of $Sirt1^{F/F}$ mice (Fig. 1C,D). In addition, although histological analysis of the testis did not show any obvious defects, the diameters of round seminiferous tubules in $Sirt1^{F/F}$*; Tnap-Cre* mice were smaller than in $Sirt1^{F/F}$ mice (Fig. 1E,F).

Sirt1 is not essential to mitosis and meiosis during spermatogenesis

Cre recombinase is expressed in primordial germ cells in $Sirt1^{F/F}$*; Tnap-Cre* mice. Therefore, to investigate the mechanism underlying the subfertility of $Sirt1^{F/F}$*; Tnap-Cre* male mice, we first examined the germ cells by immunostaining promyelocytic leukaemia zinc-finger protein (PLZF; also known as Zbtb16), which is a marker for early spermatogonial stem cells (SSCs). The number and distribution of PLZF-positive cells were comparable in $Sirt1^{F/F}$*;*

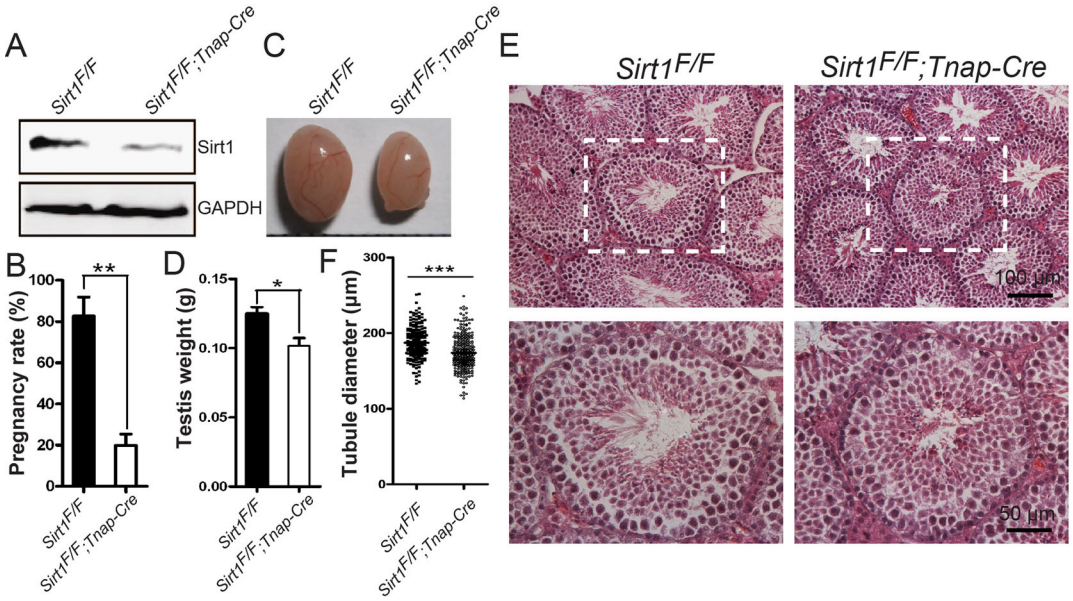

Fig. 1. Germ cell-specific *Sirt1* knockout leads to severe reproductive defects in male mice. (A) Sirt1 protein level was dramatically reduced in the testes of $Sirt1^{F/F}$*; Tnap-Cre* mice. (B) Fertility test showed that 82.67±9.15% of the plugged females became pregnant after crossing with $Sirt1^{F/F}$ males, whereas only 19.87±5.37% of the plugged females became pregnant after crossing with $Sirt1^{F/F}$*; Tnap-Cre* males. (C) Testes of 8-week-old $Sirt1^{F/F}$ and $Sirt1^{F/F}$*; Tnap-Cre*. (D) The testes of $Sirt1^{F/F}$*; Tnap-Cre* mice (0.125±0.005 g) were smaller than those of $Sirt1^{F/F}$ mice (0.102±0.006 g). (E) The histology of the seminiferous tubules of $Sirt1^{F/F}$ and $Sirt1^{F/F}$*; Tnap-Cre* mice. The boxed regions are magnified beneath. (F) The diameter of the seminiferous tubules of $Sirt1^{F/F}$*; Tnap-Cre* mice (187.3±1.53 μm) was less than that of $Sirt1^{F/F}$ mice (174.0±1.30 μm). Data are presented as mean±s.e.m. **P*<0.05, ***P*<0.01, ****P*<0.001.

Development (2017) 144, 441-451 doi:10.1242/dev.147074

Tnap-Cre and *Sirt1*$^{F/F}$ mice (Fig. S2A), indicating that SSCs were not obviously affected by Sirt1 deletion in testis. In addition, compared with *Sirt1*$^{F/F}$ mice, Sertoli cells in *Sirt1*$^{F/F}$*; Tnap-Cre* mice also showed no significant defect when assessed by immunostaining of the Sertoli cell marker Wt1 (Fig. S2B).

Meiotic progression was examined by immunostaining the axial element component of the synaptonemal complex with SYCP3 and other marker proteins. Immunostaining of SYCP3 and γH2Ax in leptotene spermatocytes revealed that double-strand break (DSB) formation was initiated in both *Sirt1*$^{F/F}$ and *Sirt1*$^{F/F}$*; Tnap-Cre* spermatocytes (Fig. S2C). Early recombination nodules (RAD51 foci) were recruited to the chromatin (Fig. S2D), and γH2Ax signals specifically accumulated in the XY body region in pachytene spermatocytes (Fig. S2C), suggesting that both *Sirt1*$^{F/F}$ and *Sirt1*$^{F/F}$*; Tnap-Cre* spermatocytes accomplished the repair process. After repair, homologue synapsis was examined by immunostaining of the synaptonemal complex protein SYCP1, which is loaded only to the synapsed chromosomes (Meuwissen et al., 1992). SYCP1 colocalized with SYCP3 (except on XY chromosomes) in most of the pachytene spermatocytes (Fig. S2E), indicating that full synapsis was acquired in the spermatocytes of *Sirt1*$^{F/F}$ and *Sirt1*$^{F/F}$*; Tnap-Cre* mice. Furthermore, the destined chiasmata marker MLH1 accumulated in pachytene stage spermatocytes of both *Sirt1*$^{F/F}$ and *Sirt1*$^{F/F}$*; Tnap-Cre* mice (Fig. S2F), and the number of MLH1 foci per cell was comparable between the two groups (Fig. S2G).

We conclude that Sirt1 is not essential to the mitotic and meiotic progression of germ cells during spermatogenesis. Thus, it might be the subsequent spermiogenesis stage that is affected in the subfertile *Sirt1*$^{F/F}$*; Tnap-Cre* mice.

Sirt1$^{F/F}$*; Tnap-Cre* mice produce round-headed spermatozoa

To investigate whether the absence of Sirt1 impairs spermiogenesis, we first examined the cauda epididymis by histological analysis. In *Sirt1*$^{F/F}$*; Tnap-Cre* mice, abnormal spermatozoa were found and sperm density was decreased in the cauda epididymis compared with *Sirt1*$^{F/F}$ mice (Fig. 2A). Quantitative analysis showed that the total number of spermatozoa in the cauda epididymis was dramatically reduced in *Sirt1*$^{F/F}$*; Tnap-Cre* compared with *Sirt1*$^{F/F}$ mice ($3.18\pm1.12\times10^6$ versus $22.15\pm0.73\times10^6$; Fig. 2B). In addition, sperm motility, as measured by computer-assisted semen analysis (CASA), was severely decreased compared with *Sirt1*$^{F/F}$ mice (10.80±0.53% versus 91.33±0.49%; Fig. 2C). All other parameters that we assessed also showed severe defects in *Sirt1*$^{F/F}$*; Tnap-Cre* compared with *Sirt1*$^{F/F}$ mice (Fig. 2D-G), including the percentage of progressive spermatozoa (1.27±0.12% versus 21.17±0.65%), average path velocity (VAP; 16.10±0.20 µm/s versus 93.22±1.41 µm/s), straight line velocity (VSL; 14.15±0.13 µm/s versus 60.90±1.34 µm/s) and curvilinear velocity (VCL; 37.36±0.55 µm/s versus 181.0±1.95 µm/s). Further morphological evaluation found that in *Sirt1*$^{F/F}$*; Tnap-Cre* mice, many spermatozoa had irregularly shaped or round heads (Fig. 2H,J). This phenotype is very similar to that found in human globozoospermia, a serious fertility disorder that is characterized by round-headed spermatozoa with malformed or absent acrosomes (Dam et al., 2007). To examine whether the absence of Sirt1 impairs acrosomes, we examined the single-sperm immunofluorescence of Sp56 (Zp3r), an acrosome-specific marker. In *Sirt1*$^{F/F}$ mice, most spermatozoan acrosomes exhibited a typical crescent moon shape (Fig. 2I). By contrast, the acrosomes of *Sirt1*$^{F/F}$*; Tnap-Cre* mice exhibited various defects, including deformation, mislocalization and fragmentation. Transmission electron microscopy (TEM) analysis of the cauda epididymis in Sirt1-deficient mice also showed malformed acrosomes (Fig. 2K). Together, these findings suggest that Sirt1 might be involved in acrosome formation and the pathogenesis of globozoospermia.

Abnormal acrosome biogenesis in *Sirt1*$^{F/F}$*; Tnap-Cre* mice

To characterize and confirm the defects in acrosome formation in *Sirt1*$^{F/F}$*; Tnap-Cre* mice, TEM analysis was performed. In *Sirt1*$^{F/F}$ mice, all four acrosome biogenesis phases, including Golgi phase, cap phase, acrosome phase and maturation phase (Abou-Haila and Tulsiani, 2000), could be identified by their standard characteristics (Fig. 3A,C,E,G). However, in *Sirt1*$^{F/F}$*; Tnap-Cre* mouse testis, multiple acrosomal structures could be detected in both Golgi phase and cap phase (Fig. 3B,D). These results suggest that the malformed acrosomes in *Sirt1*$^{F/F}$*; Tnap-Cre* mice might result from the failure of proacrosomal vesicles to fuse or to be transported to the preacrosomal structure. In the subsequent stages of acrosome biogenesis, vacuolated or irregularly shaped acrosomes were observed in the acrosome phase and maturation phase of Sirt1-deficient spermatids (Fig. 3F,H). Together, these results indicate that acrosome biogenesis was affected in *Sirt1*$^{F/F}$*; Tnap-Cre* mice.

To further examine how *Sirt1* knockout affects acrosome biogenesis, the acrosome was labelled with an antibody against Sp56 at the early stages of spermiogenesis. As shown in Fig. 4A, a single acrosomal vesicle was attached to one end of the nucleus in *Sirt1*$^{F/F}$ spermatids, indicating that proacrosomal vesicles derived from the Golgi apparatus were fused. By contrast, in *Sirt1*$^{F/F}$*; Tnap-Cre* mice, fragmented or unfused Sp56-positive structures were observed in the perinuclear region, and ∼20% of the spermatids were observed with multiple small vesicles without fusing (Fig. 4B), which was similar to observations from TEM analysis. These results indicate that Sirt1 is involved in the transportation/fusion of Golgi-derived proacrosomal vesicles to form the nucleus-associated acrosome.

Previously, we found that autophagy is involved in acrosome biogenesis and that the autophagic molecular marker microtubule-associated protein light chain (LC3; also known as Map1lc3a) localizes on Golgi apparatus-derived vesicles (Wang et al., 2014). We examined the localization of LC3 and its relationship with Golgi apparatus-derived vesicles by immunofluorescence labelling of LC3 and TGN38 (a *trans*-Golgi network marker; also known as Tgoln1/2). At the early stages of spermiogenesis in *Sirt1*$^{F/F}$ mice, LC3 colocalized with TGN38 in spermatids (Fig. 4C). This colocalization was significantly reduced in *Sirt1*$^{F/F}$*; Tnap-Cre* mice (Fig. 4C,D). These data suggested that LC3 transfer to the Golgi-derived vesicles was affected in Sirt1-deficient testes. Interestingly, in *Sirt1*$^{F/F}$*; Tnap-Cre* mice, Sirt1 deficiency in germ cells led to an accumulation of LC3 in the nucleus (Fig. 4C,E), and some spermatids with LC3 in the nucleus showed no colocalization between LC3 and TGN38 (Fig. 4C), thus indicating that the nuclear accumulation of LC3 might affect proacrosomal granule fusion or the delivery of the granules to the nucleus-associated acrosomal vesicles.

Autophagic flux is partially disrupted in the testis of *Sirt1*$^{F/F}$*; Tnap-Cre* mice

Recently, it was reported that LC3 can be deacetylated by Sirt1 in the nucleus, which mediates the redistribution of LC3 to the cytoplasm, where it can conjugate to Atg7 and drive autophagy initiation (Huang et al., 2015). To test whether the nucleocytoplasmic distribution of LC3 in spermatids is regulated by Sirt1, the acetylation status of LC3 in testis was determined by immunoprecipitation with an antibody to LC3 followed by western blotting with an anti-acetyl-lysine antibody. As shown in Fig. 5A, compared with *Sirt1*$^{F/F}$ mice, the acetylation of LC3 in testis was obviously increased after Sirt1 deletion in the *Sirt1*$^{F/F}$*; Tnap-Cre*

Development (2017) 144, 441-451 doi:10.1242/dev.147074

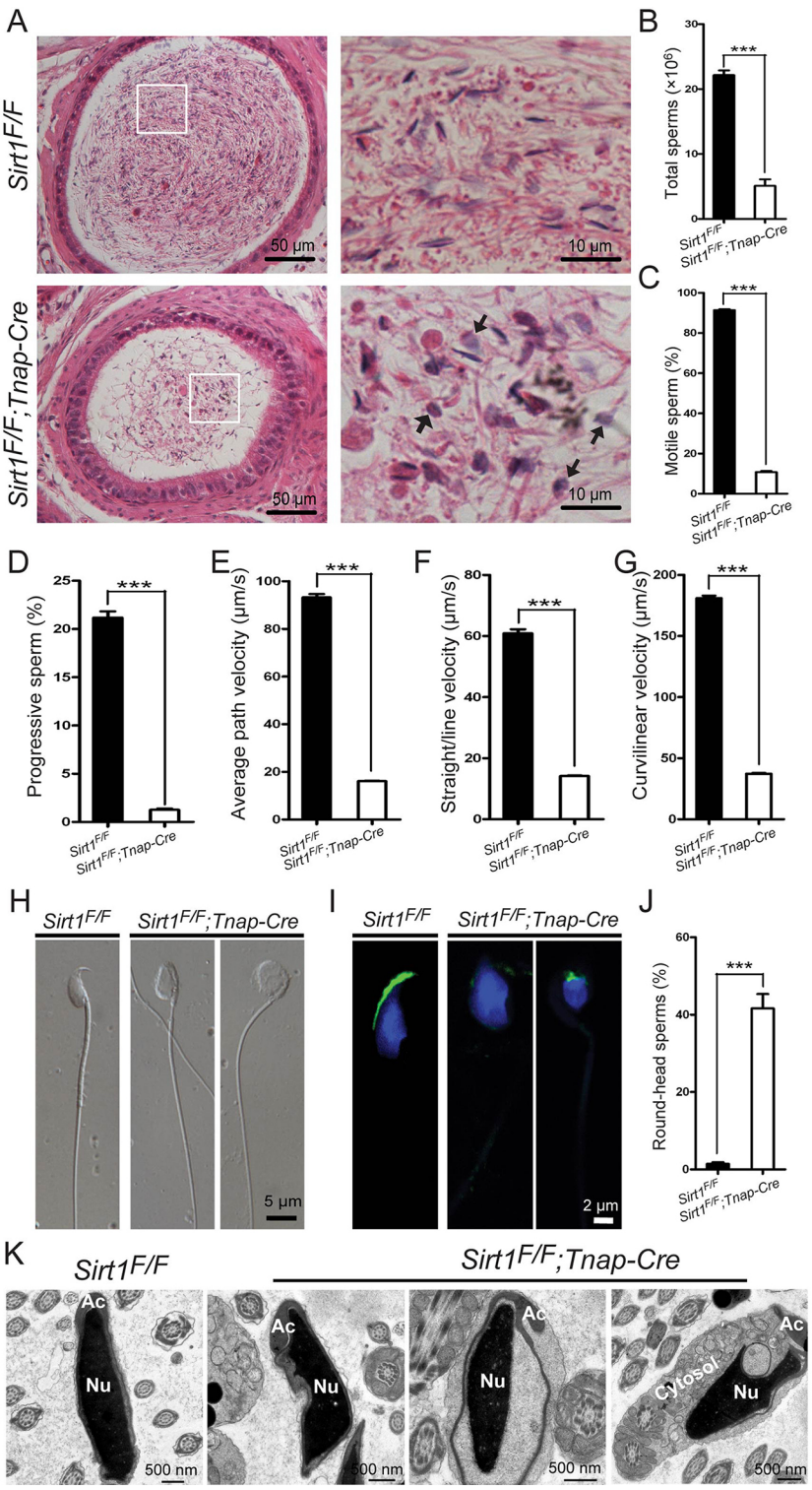

Fig. 2. Defects of *Sirt1$^{F/F}$; Tnap-Cre* spermatozoa. (A) Histology of the cauda epididymis of *Sirt1$^{F/F}$* and *Sirt1$^{F/F}$; Tnap-Cre* mice. Boxed regions are magnified to the right. Arrows indicate abnormal spermatozoa. (B) The total number of sperm in *Sirt1$^{F/F}$; Tnap-Cre* cauda epididymis ($3.18\pm1.12\times10^6$) was significantly reduced compared with that of *Sirt1$^{F/F}$* mice ($22.15\pm0.73\times10^6$). (C) Motile sperm in *Sirt1$^{F/F}$* (91.33±0.49%) and *Sirt1$^{F/F}$; Tnap-Cre* (10.80±0.53%) mice. (D) Progressive sperm in *Sirt1$^{F/F}$* (21.17±0.65%) and *Sirt1$^{F/F}$; Tnap-Cre* (1.27±0.12%) mice. (E) The average path velocity (VAP) of sperm from *Sirt1$^{F/F}$* (93.22±1.41 μm/s) and *Sirt1$^{F/F}$; Tnap-Cre* (16.10±0.20 μm/s) mice. (F) The straight line velocity (VSL) of sperm from *Sirt1$^{F/F}$* mice (60.90±1.34 μm/s) and *Sirt1$^{F/F}$; Tnap-Cre* (14.15±0.13 μm/s) mice. (G) The curvilinear velocity (VCL) of sperm from *Sirt1$^{F/F}$* (181.0±1.95 μm/s) and *Sirt1$^{F/F}$; Tnap-Cre* (37.36±0.55 μm/s) mice. (H) Confocal images showing round-headed spermatozoa in *Sirt1$^{F/F}$; Tnap-Cre* mice. (I) Defects of the acrosome in *Sirt1$^{F/F}$; Tnap-Cre* mice. Acrosomes were visualized by immunofluorescence of the acrosome-specific marker Sp56 (green); nucleus is in blue. (J) The percentage of abnormal spermatozoa with globozoospermia-like morphology was higher in *Sirt1$^{F/F}$; Tnap-Cre* (41.60±3.71%) than in *Sirt1$^{F/F}$* (1.41±0.43%) mice. Data are presented as the mean±s.e.m. ***P<0.001. (K) TEM analysis of spermatozoa from *Sirt1$^{F/F}$* and *Sirt1$^{F/F}$; Tnap-Cre* cauda epididymis. The *Sirt1$^{F/F}$;Tnap-Cre* images illustrate spermatozoa with an irregular acrosome (left), with a separate acrosome (middle) or with cytoplasm (right). Nu, nucleus; Ac, acrosome.

mice; this explains the accumulation of acetylated LC3 in the nucleus of the spermatids. As Sirt1 could interact with and deacetylate several essential components of the autophagy machinery, such as Atg5 and Atg7, to modulate the autophagy processes (Lee et al., 2008), we assessed the acetylation status of Atg7 in germ cells using acetyl-lysine immunoprecipitation followed by western blotting with an anti-Atg7 antibody. We found that the acetylation of Atg7 in *Sirt1$^{F/F}$; Tnap-Cre* mice dramatically increased compared with *Sirt1$^{F/F}$* mice (Fig. 5B). Thus, Sirt1 might regulate the activation of autophagy by modulating the acetylation status of LC3 and Atg7 in testis.

Sirt1 might be involved in acrosome biogenesis through the modulation of autophagy. To test this, we first evaluated the effect of Sirt1 deficiency on autophagic flux in the testis. Immunoblotting analysis showed that the total levels of the autophagic substrate SQSTM1 (p62) were clearly elevated in the testis of *Sirt1$^{F/F}$; Tnap-Cre* compared with *Sirt1$^{F/F}$* mice (Fig. 5C); the unconjugated LC3 form was also slightly increased (Fig. 5C), and a similar SQSTM1

Development (2017) 144, 441-451 doi:10.1242/dev.147074

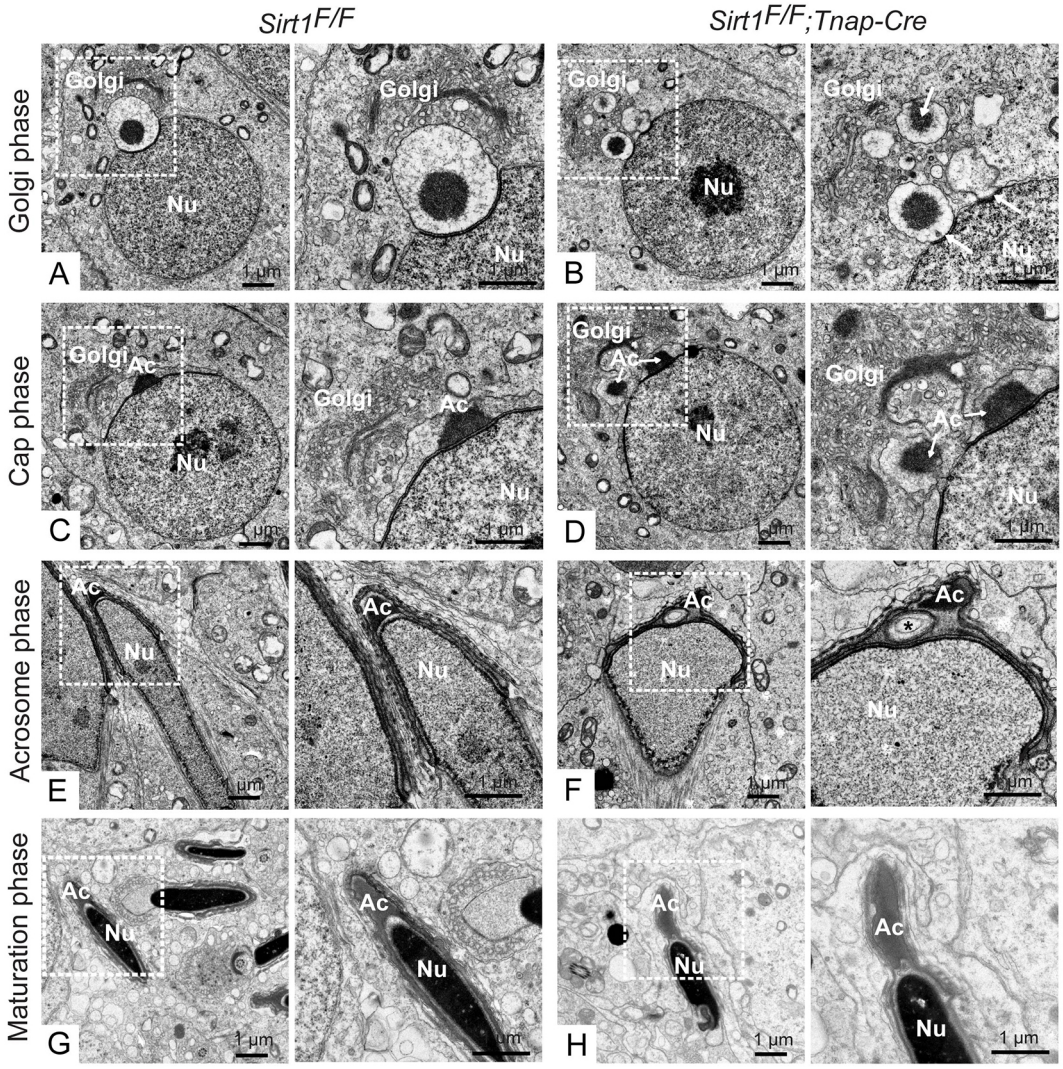

Fig. 3. Ultrastructural analysis of acrosome biogenesis in *Sirt1*$^{F/F}$ and *Sirt1*$^{F/F}$*; Tnap-Cre* mice. (A,B) The ultrastructures of Golgi phase from *Sirt1*$^{F/F}$ and *Sirt1*$^{F/F}$*; Tnap-Cre* mouse testis, showing three proacrosomal centres (arrows) around the nucleus in *Sirt1*$^{F/F}$*; Tnap-Cre* testis. (C,D) Cap phase, showing that there were two additional acrosomal structures (arrows) around the nucleus in *Sirt1*$^{F/F}$*; Tnap-Cre* mouse testis. (E,F) Acrosome phase, showing that there were vacuolated (asterisks) or irregularly shaped acrosomes in *Sirt1*$^{F/F}$*; Tnap-Cre* spermatids. (G,H) Maturation phase, showing irregularly shaped acrosomes in *Sirt1*$^{F/F}$*; Tnap-Cre* spermatids. Boxed regions are magnified to the right. Nu, nucleus; Ac, acrosome.

accumulation was also observed by immunofluorescence (Fig. 5D,E). To confirm this defect, we performed TEM analysis in testis. The large double-membrane vacuoles filled with cargos could be detected in *Sirt1*$^{F/F}$ mouse testes (Fig. 5F, upper panel), which is the typical appearance of autolysosomes (Eskelinen et al., 2011; Gerland et al., 2004). However, in the *Sirt1*$^{F/F}$*; Tnap-Cre* mice, only a few electron-dense lysosomes surrounded by some unfused small vesicles were observed (Fig. 5F, lower panel), and few autophagosomes were found in these spermatids (Klionsky and Eskelinen, 2014). These results indicate that autophagic flux is partially disrupted in the germ cells of Sirt1-deficient mice.

GOPC and PICK1 fail to be recruited to the acrosome in Sirt1-deficient germ cells

To examine whether the absence of Sirt1 affects the transportation/fusion of several acrosome biogenesis-related proteins during formation of the nucleus-associated acrosome, the localization of GOPC (golgi associated PDZ and coiled-coil motif containing protein), beclin 1 (an autophagy-related protein; also known as Atg6) and Sp56 was examined in the spermatids by immunofluorescence. GOPC is proposed to be involved in vesicle trafficking from the Golgi apparatus to the acrosome and interacts with beclin 1 (Yao et al., 2002; Wang et al., 2014). As shown in Fig. 6A, in both *Sirt1*$^{F/F}$ and *Sirt1*$^{F/F}$*; Tnap-Cre* mice, beclin 1 predominately colocalized with Sp56. GOPC colocalized with beclin 1 in the acrosomal region in round spermatids of *Sirt1*$^{F/F}$ mice but failed to be recruited to the acrosomal region of *Sirt1*$^{F/F}$*; Tnap-Cre* mice. Statistical analysis showed that GOPC and Sp56 colocalization was significantly reduced in *Sirt1*$^{F/F}$*; Tnap-Cre* mice (48.77±5.28%) compared with *Sirt1*$^{F/F}$ mice (81.63±2.49%) (Fig. 6B); this suggests that GOPC fails to be recruited to the acrosome in Sirt1-deficient germ cells.

We then examined the localization of another GOPC-associated protein, PICK1, which is a highly expressed peripheral membrane protein in round spermatids that is localized to Golgi-derived proacrosomal granules (Xiao et al., 2009) according to immunofluorescence studies. PICK1 predominately colocalized with Sp56 in *Sirt1*$^{F/F}$ mice Fig. 6C. By contrast, many PICK1

Development (2017) 144, 441-451 doi:10.1242/dev.147074

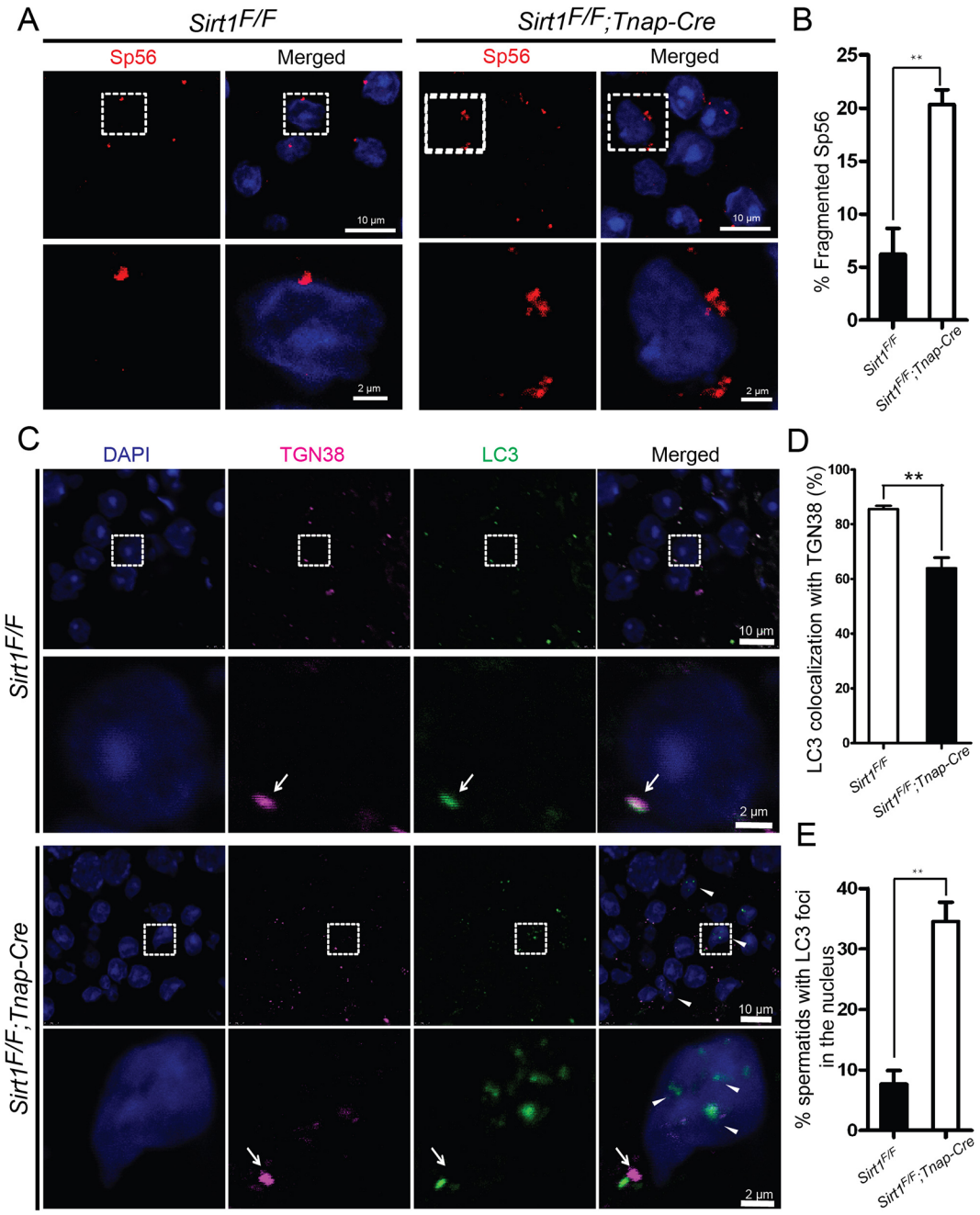

Fig. 4. Abnormal acrosomal biogenesis of *Sirt1*$^{F/F}$*; Tnap-Cre* mice. (A) Sp56 immunofluorescence (red) of *Sirt1*$^{F/F}$ and *Sirt1*$^{F/F}$*; Tnap-Cre* testes. Fragmented acrosomes were observed in the *Sirt1*$^{F/F}$*; Tnap-Cre* spermatids. Blue indicates nuclei (DAPI). Boxed regions are magnified beneath. (B) Quantification of spermatids with fragmented acrosomes: *Sirt1*$^{F/F}$, 6.20±2.44%; *Sirt1*$^{F/F}$*; Tnap-Cre*, 20.33±1.39%. (C) Immunodetection of LC3 (green) and TGN38 (pink) colocalization in the seminiferous tubules of *Sirt1*$^{F/F}$ and *Sirt1*$^{F/F}$*; Tnap-Cre* mice. TGN38 and LC3 colocalized (arrows) in *Sirt1*$^{F/F}$ spermatids but not in those of *Sirt1*$^{F/F}$*; Tnap-Cre* mice. There was more LC3 in the nucleus (arrowheads) of the spermatids of *Sirt1*$^{F/F}$*; Tnap-Cre* mice than in those of *Sirt1*$^{F/F}$ mice. (D) Statistical analysis of LC3 and TGN38 colocalization in the spermatids of *Sirt1*$^{F/F}$ and *Sirt1*$^{F/F}$*; Tnap-Cre* mice: *Sirt1*$^{F/F}$, 85.51±1.21%; *Sirt1*$^{F/F}$*; Tnap-Cre*, 63.90±3.88%. (E) Statistical analysis of spermatids with LC3 foci in the nucleus: *Sirt1*$^{F/F}$, 7.71±2.21%; *Sirt1*$^{F/F}$*; Tnap-Cre*, 34.57±3.13%. Data are presented as mean±s.e.m. $^{**}P<0.01$.

molecules failed to be recruited to the acrosomal region in the spermatids of *Sirt1*$^{F/F}$*; Tnap-Cre* mice (Fig. 6C,D).

Taken together, these findings indicate that the acrosome biogenesis defect in *Sirt1*$^{F/F}$*; Tnap-Cre* mice might be due to a failure to recruit GOPC and PICK1 to nucleus-associated acrosomal vesicles.

DISCUSSION

Sirt1 has multiple physiological functions, most of which are dependent on the acetylation status of specific substrates (Haigis and Guarente, 2006; Martinez-Redondo and Vaquero, 2013; Saunders and Verdin, 2007). Given that Sirt1 is induced by calorie restriction and that Sirt1 activity is necessary for the induction of starvation-induced autophagy (Lee et al., 2008), the relationship between Sirt1 and autophagy has been known for some years (Cui et al., 2006; Kume et al., 2010; Ng and Tang, 2013; Zeng et al., 2012). Sirt1 co-immunoprecipitates with Atg5, Atg7 and LC3/LC3b (Map1lc3b or Atg8), thereby establishing the connection between Sirt1 and autophagy (Lee et al., 2008). Under starvation conditions, Atg5,

Development (2017) 144, 441-451 doi:10.1242/dev.147074

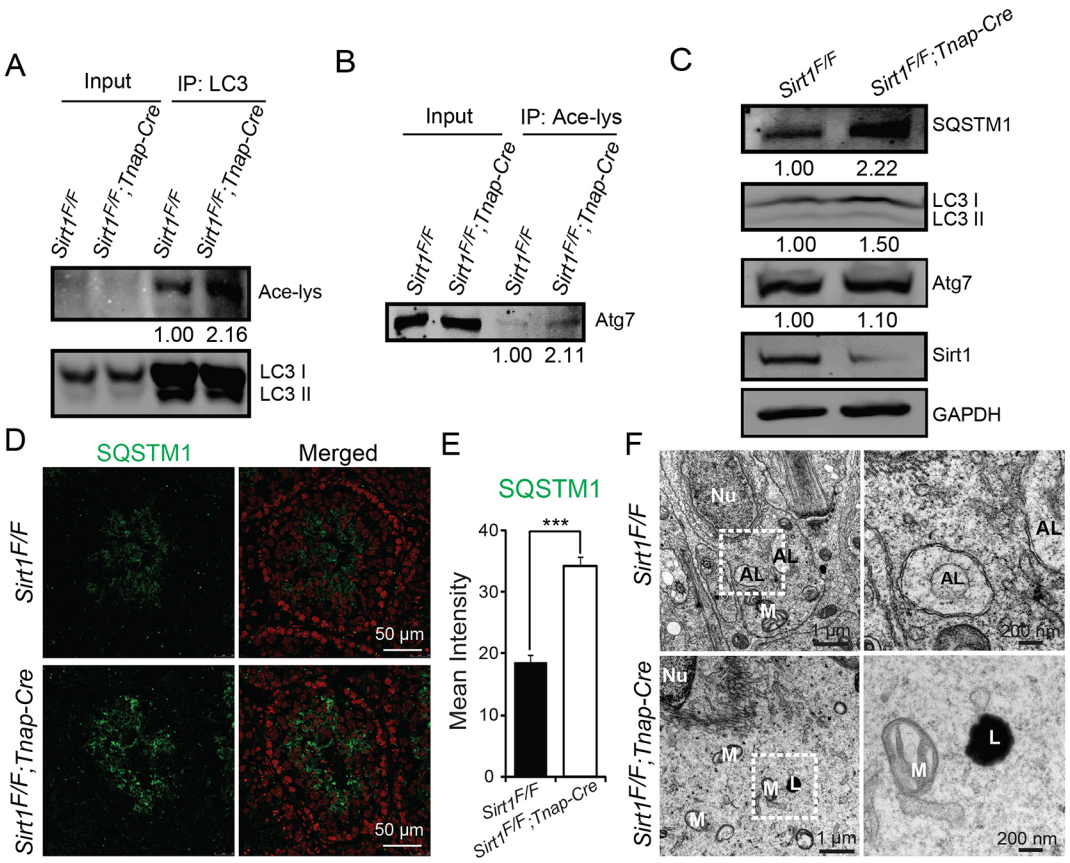

Fig. 5. Autophagic flux is disrupted in the germ cells of male *Sirt1$^{F/F}$; Tnap-Cre* mice. (A) Acetylation of endogenous LC3 in the testes of *Sirt1$^{F/F}$* and *Sirt1$^{F/F}$; Tnap-Cre* mice, as detected by immunoprecipitation with an anti-LC3 antibody. The immunocomplexes were analyzed by western blotting with an anti-acetyl-lysine antibody. Numbers refer to relative amounts of acetylated LC3 (quantified using Odyssey software). (B) Acetylation of endogenous Atg7 in the germ cells of *Sirt1$^{F/F}$* and *Sirt1$^{F/F}$; Tnap-Cre* mice, as detected by immunoprecipitation with an anti-acetyl-lysine antibody. The immunocomplexes were analyzed by western blotting with an anti-Atg7 antibody. Relative amounts of acetylated Atg7 are indicated. (C) Immunoblotting analysis of SQSTM1 (p62), LC3 and Atg7 in the testes of *Sirt1$^{F/F}$* and *Sirt1$^{F/F}$; Tnap-Cre* mice. Relative amounts of acetylated SQSTM1, LC3I and Atg7 are indicated. (D) Immunofluorescence detection of SQSTM1 (green) in the seminiferous tubules of *Sirt1$^{F/F}$* and *Sirt1$^{F/F}$; Tnap-Cre* mice. Red, nuclei (PI). (E) Quantification of the fluorescence intensity of SQSTM1 in D. Data are presented as mean±s.e.m. ***P<0.001. (F) Ultrastructural analysis of *Sirt1$^{F/F}$* and *Sirt1$^{F/F}$; Tnap-Cre* spermatids. Boxed regions are magnified to the right. Nu, nucleus; AL, autolysosome; M, mitochondria.

Atg7 and LC3b can be deacetylated by Sirt1 (Lee et al., 2008); the deacetylation of LC3 by Sirt1 in the nucleus is a prerequisite for LC3 redistribution to the cytoplasm, and the nucleocytoplasmic transport of LC3 is essential for autophagosome formation (Huang et al., 2015). However, until now, the biological relevance of LC3 nucleocytoplasmic transportation has largely remained unexplored. Here, we show that the depletion of Sirt1 in germ cells leads to the accumulation of acetylated LC3 in the nucleus and to a partial disruption of autophagic flux in spermatids. Thus, it is possible that during spermiogenesis Sirt1 deacetylates LC3 in the nucleus, thereby mediating LC3 nucleocytoplasmic transport. Once in the cytoplasm, LC3 is activated by Atg7 and is then transferred to Golgi-derived vesicles to promote acrosome biogenesis (Fig. 7). Therefore, our investigations discovered a novel physiological function for Sirt1-mediated LC3 nucleocytoplasmic transportation in the biogenesis of a spermatozoa-specific organelle. In addition, Sirt1 could regulate the acetylation status of Atg7 in testis, and our previous work also indicated that Atg7 is required for acrosome biogenesis during spermatogenesis in mice (Wang et al., 2014). Thus, Sirt1 might participate in acrosome biogenesis through the autophagy pathway. The germ cell-specific *Sirt1* knockout mice had abnormal spermatozoa, with irregularly shaped or rounded heads and less acrosome (Fig. 2H,J), which was very similar to the round-headed spermatozoa with malformed acrosome characteristic of human globozoospermia (Dam et al., 2007). The proportion of round-headed spermatozoa in Sirt1-deficient mice was 41.60± 3.71%, which is similar to partial globozoospermia (Dam et al., 2011), suggesting *Sirt1* as a potential globozoospermia pathogenic gene. The partial globozoospermia phenotype might result from either the activation of alternative pathways or gene redundancy.

In addition to acrosome biogenesis defects, we observed a decrease in sperm count; this appears to be a common phenotype for a variety of genetic defects that perturb the normal programme of mouse spermiogenesis (Kang-Decker et al., 2001; Venables and Cooke, 2000; Wang et al., 2014). Bell et al. (2014) found that the histone to protamine transition was disrupted in Sirt1-deficient spermatids, and this might partially account for the decrease in sperm count. An alternative explanation relates to the functional diversity of Sirt1 during spermatogenesis. In the testis of *Sirt1$^{F/F}$; Tnap-Cre* mice, we observed many TUNEL signals in the germ cells (Fig. S3), which was consistent with the findings of some previous studies (Bell et al., 2014; Kolthur-Seetharam et al., 2009). In yeast, Sir2 can inhibit ribosomal DNA recombination and relocalize to the sites of DNA breaks; the absence of Sir2 activity leads to silencing defects, sensitivity to DNA damage and increased genomic instability (Denu, 2003; Guarente and Picard, 2005). In mammalian cells, Sirt1 promotes DNA repair by

Development (2017) 144, 441-451 doi:10.1242/dev.147074

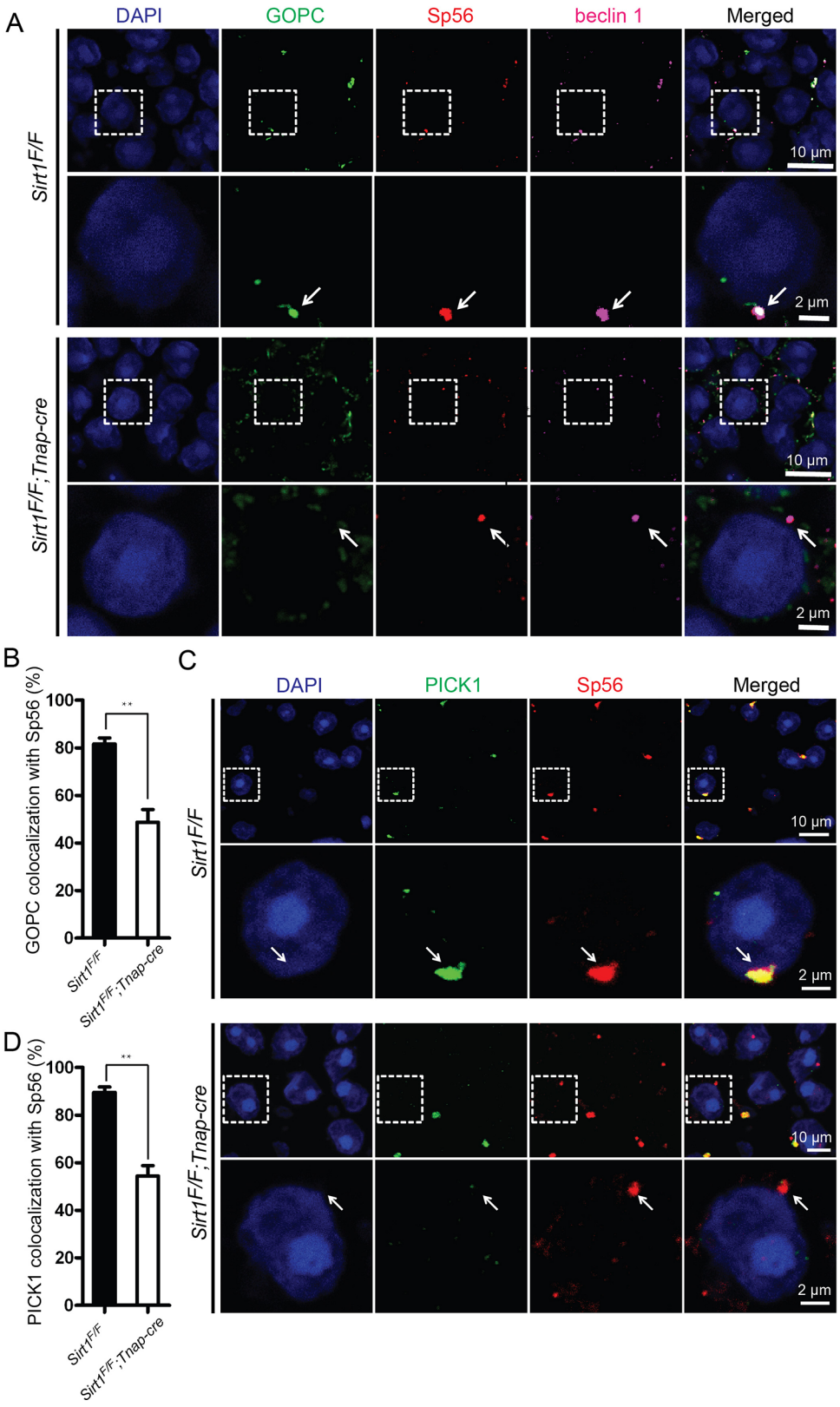

Fig. 6. GOPC and PICK1 fail to be recruited to the acrosome in *Sirt1*$^{F/F}$; *Tnap-Cre* spermatids. (A) GOPC (green), Sp56 (red) and beclin 1 (pink) colocalized (arrows) in the spermatids of *Sirt1*$^{F/F}$ mice. Sp56 and beclin 1 still colocalized in *Sirt1*$^{F/F}$; *Tnap-Cre* spermatocytes, but GOPC (green) was not recruited to the acrosome. Boxed regions are magnified beneath. (B) Statistical analysis of GOPC and Sp56 colocalization in *Sirt1*$^{F/F}$ and *Sirt1*$^{F/F}$; *Tnap-Cre* mice: *Sirt1*$^{F/F}$, 81.63±2.49%; *Sirt1*$^{F/F}$; *Tnap-Cre*, 48.77±5.28%. (C) The colocalization of Sp56 and PICK1 was disrupted in the germ cells of *Sirt1*$^{F/F}$; *Tnap-Cre* mice. (D) Statistical analysis of PICK1 and Sp56 colocalization in *Sirt1*$^{F/F}$ and *Sirt1*$^{F/F}$; *Tnap-Cre* mice: *Sirt1*$^{F/F}$, 89.56 ±2.22%; *Sirt1*$^{F/F}$; *Tnap-Cre*, 54.40±4.35%. Data are mean±s.e.m. $^{**}P<0.01$.

deacetylating various DNA repair factors, including Nijmegen breakage syndrome protein 1 (NBS1; also known as nibrin) (Yuan et al., 2007), Werner syndrome protein (WRN) (Lee et al., 2015), Ku70 (Xrcc6) (Jeong et al., 2007), xeroderma pigmentosum complementation group A (XPA) (Fan and Luo, 2010) and Krüppel-associated box (KRAB)-associated protein 1 (KAP1; also known as Trim28) (Lin et al., 2015). In addition, Sirt1 can be recruited to DSBs in an ATM-dependent manner, and deacetylates and stimulates HDAC1, thus facilitating the dynamic regulation of HDAC1 activity, which is essential for DSB repair through non-homologous end joining (Dobbin et al., 2013). The role of Sirt1 in DNA repair has been substantiated in *Sirt1*$^{-/-}$ embryos, which exhibit

Development (2017) 144, 441-451 doi:10.1242/dev.147074

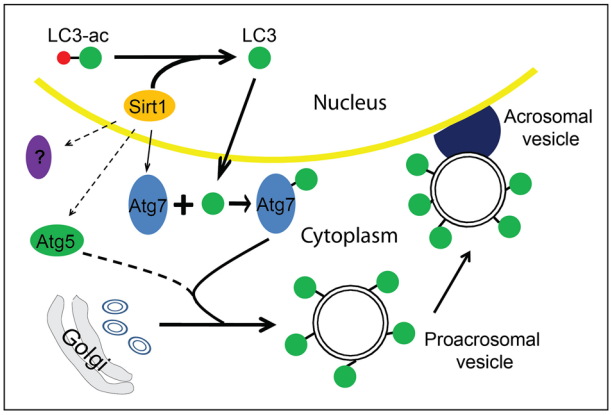

Fig. 7. Model for the role of Sirt1 in acrosome biogenesis. Sirt1 can deacetylate LC3 and Atg7 (solid line) or other autophagic components (dashed line). The deacetylated LC3 is then transferred to the cytoplasm, where it interacts with autophagic effectors and initiates autophagy. The deacetylated Atg7 (or some other autophagic components) activates autophagy. The entire autophagic machinery participates in the fusion and transportation of Golgi-derived proacrosomal vesicles to the acrosome to promote acrosome biogenesis.

increased chromosomal aberrations and impaired DNA repair (Wang et al., 2008). Because most of the above-mentioned molecules are involved in meiotic recombination, it is likely that cell death in the tubule lumens of the testes is dependent on impaired meiotic recombination after Sirt1 depletion. This indicates that Sirt1 might be involved in more than one process during spermatogenesis.

In the *Sirt1*$^{F/F}$*; Tnap-Cre* mice, several characteristic phenotypes of *Sirt1*$^{-/-}$ mice (including a small, feeble body with significantly increased post-natal mortality rates) disappeared, and only defects in spermiogenesis (mainly malformed spermatozoa) were observed. This indicates that Sirt1 performs various functions that are dependent on cell type or developmental stage.

Taken together, our findings demonstrate that the malformed spermatozoa defects in *Sirt1*$^{-/-}$ mice were mainly caused by a deficiency of Sirt1 in germ cells rather than in steroidogenic cells, and impaired acrosome biogenesis might be the main cause of the observed male infertility. Further investigation revealed that Sirt1 can deacetylate nuclear LC3, and the deacetylated LC3 is then transported to the cytoplasm, where it interacts with autophagic effectors and initiates autophagy. After this sequence of events, the entire autophagic molecular machinery participates in the fusion and transportation of Golgi-derived proacrosomal vesicles to the acrosome (Fig. 7). In conclusion, our research describes a novel mechanism for the regulation of acrosome biogenesis through Sirt1-mediated LC3 nucleocytoplasmic transportation.

MATERIALS AND METHODS

Mice

Sirt1$^{F/F}$*; SF1-Cre* mice were bred from *Sirt1*$^{F/F}$ mice (Jackson Laboratory) and the *SF1-Cre* mouse strain (Jackson Laboratory). *Sirt1*$^{F/F}$*; Tnap-Cre* mice were bred from *Sirt1*$^{F/F}$ mice and *Tnap-Cre* mice (Jackson Laboratory, 008569). Mice were maintained under controlled environmental conditions with free access to food and water, and illumination was provided between 08:00 and 20:00. All animal experiments were approved by the Animal Research Panel of the Committee on Research Practice of the University of Chinese Academy of Sciences.

Antibodies

Rabbit anti-LC3 polyclonal antibody (ab58610, 1:200), sheep anti-beclin 1 polyclonal antibody (ab62108, 1:100), rabbit anti-SYCP3 polyclonal antibody (ab15093, 1:200) and rabbit anti-GOPC antibody (ab37036, 1:100) were purchased from Abcam. Sheep anti-TGN38 polyclonal antibody (NB110-60519, 1:200), rabbit anti-SYCP1 polyclonal antibody-Cy5 (NB300-228c, 1:100) and chicken anti-PICK1 (NBP1-42829, 1:200) were purchased from Novus Biologicals. Mouse anti-γH2Ax monoclonal antibody (05-636, 1:200) was from Merck Millipore, and mouse anti-MLH1 monoclonal antibody (51-1327GR, 1:100) was from BD Pharmingen. Mouse anti-SYCP3 monoclonal antibody (SC-74569, 1:200), rabbit anti-RAD51 polyclonal antibody (SC-8349, 1:100) and rabbit anti-Sirt1 polyclonal antibody (SC-15404, 1:500) were purchased from Santa Cruz Biotechnology. Mouse anti-Sp56 (55101, 1:200) antibody was purchased from QED Bioscience. Mouse anti-acetylated-lysine monoclonal antibody (9681, 1:500 for western blotting), rabbit anti-acetylated-lysine polyclonal antibody (9441, 1:100 for immunoprecipitation) and rabbit anti-SQSTM1 polyclonal antibody (5114, 1:500 for western blotting and 1:100 for immunofluorescence) were purchased from Cell Signaling Technology. Mouse anti-Atg7 monoclonal antibody (SAB4200304, 1:1000) and rabbit anti-LC3 polyclonal antibody (L7543, 1:1000), which were used in western blot analysis, were purchased from Sigma-Aldrich. Goat anti-rabbit FITC, goat anti-mouse FITC, goat anti-rabbit TRITC and goat anti-mouse TRITC-conjugated secondary antibodies, as well as horseradish peroxidase (HRP)-conjugated secondary antibodies, were purchased from Zhong Shan Jin Qiao (Beijing, China). Donkey anti-rabbit Cy5 and donkey anti-sheep FITC-conjugated secondary antibodies were purchased from Jackson ImmunoResearch. Alexa Fluor 680-conjugated goat anti-mouse and Alexa Fluor 800-conjugated goat anti-rabbit secondary antibodies, which were used in western blot analysis, were purchased from Invitrogen.

Isolation and primary culture of Leydig cells

Leydig cells were isolated as previously described, with minor modifications (Svechnikova et al., 2011). Briefly, the 2-month-old mice were euthanized by cervical dislocation, and the testes were removed and washed three times with PBS. The testes were then decapsulated and incubated with 1 mg/ml collagenase IV in DMEM/F12 in a shaking water bath (120 cycles/min) at 37°C for 15 min. After incubation, cold DMEM/F12 containing 5% fetal bovine serum (FBS; 10270, Gibco) was added to stop the action of collagenase IV. Seminiferous tubules were separated from the interstitial cells by gravity sedimentation. The cells were collected by centrifugation (300 ***g*** for 6 min) and resuspended in 2 ml DMEM/F12 containing 5% FBS. To obtain purified Leydig cells, this suspension was loaded onto a discontinuous Percoll gradient consisting of layers of 30%, 40%, 50% and 60% Percoll dissolved in Hank's Balanced Salt Solution and centrifuged at 600 ***g*** at 4°C for 28 min. Leydig cells were primarily distributed from fraction 50% to 60%. Subsequently, the fraction enriched in Leydig cells was centrifuged through a continuous self-generated 60% Percoll gradient at 20,000 ***g*** for 30 min at 4°C. The purity of Leydig cell preparations was greater than 90%, as determined by histochemical staining for 3β-hydroxysteroid dehydrogenase (3β-HSD) (PAYNE et al., 1980). These purified Leydig cells were cultured in DMEM/F12 supplemented with 15% FBS, 100 IU/ml penicillin and 100 µg/ml streptomycin at 34°C and 5% CO_2.

Hormone measurement

Serum levels of mouse testosterone were measured using a radioimmunoassay kit (Beijing Sinouk Institute of Biological Technology) as previously described (Mason-Garcia et al., 1985).

Assessment of mating efficiency

Males of different genotypes (8-9 weeks) were used for mating efficiency measurement. Each male mouse was caged with two wild-type CD1 female mice (7-8 weeks) and their vaginal plugs were checked every morning. Each male underwent 10-15 cycles of the above measurement with different female mice.

Assessment of fertility

Males of different genotypes (8-9 weeks) were used for the breeding assay. Each male mouse was caged with two wild-type CD1 females (7-8 weeks) and their vaginal plugs were checked every morning. The number of pups in

Development (2017) 144, 441-451 doi:10.1242/dev.147074

each cage was counted within a week of birth. Each male underwent four cycles of the above breeding assay with different females.

Epididymal sperm count assays

Epididymal sperm count assays were performed as previously described (Jimenez et al., 2010; Kullander and Rausing, 1975). Briefly, the cauda epididymis was dissected from adult mice. Spermatozoa were squeezed from the cauda epididymis and incubated for 30 min at 37°C under 5% CO_2. The medium was then diluted 1:500 and transferred to a hemocytometer for counting. Non-fixed spermatozoa were spread on precoated slides for morphological observation or immunostaining.

Sperm motility assays

Sperm motility assays were performed as previously described (Jimenez et al., 2010; Kullander and Rausing, 1975). Briefly, the cauda epididymis was dissected from adult mice and spermatozoa were allowed to exude from incisions of the cauda epididymis for 30 min at 37°C under 5% CO_2. Then, 10 µl of the exudate was placed into a glass cell chamber (Leja Products BV, Nieuw-Vennep, The Netherlands). The chambers were maintained at 37°C on a heated platform, and the spermatozoa were viewed using an Olympus BX51 microscope through a 20× phase objective. Viewing areas on each chamber were imaged using a CCD camera (Olympus). The samples were analyzed using CASA (CEROS v.12, Hamilton Thorne Research) implemented using the Minitube Sperm Vision Digital Semen Evaluation System (12500/1300, Minitube Group, Tiefenbach, Germany). Various sperm motility parameters were analyzed, including total motility, progressive sperm, average path velocity (VAP), straight line velocity (VSL) and curvilinear velocity (VCL).

Tissue collection and histological analysis

Testes and cauda epididymides were dissected immediately following euthanization by cervical dislocation. The tissues were then fixed in 4% paraformaldehyde (PFA; pH 7.5) overnight at 4°C, dehydrated and embedded in paraffin; sections (5 µm) were cut and mounted on glass slides. Following deparaffinization, the slides were stained with Haematoxylin and Eosin (H&E) for histological analysis.

Transmission electron microscopy

Adult mouse testes were dissected and fixed with 2.5% (v/v) glutaraldehyde in 0.2 M cacodylate buffer (pH 7.4) overnight. After washing in 0.2 M cacodylate buffer, tissues were cut into pieces of ∼1 mm^3 and immersed in 1% OsO_4 for 2 h at 4°C. Then, the samples were dehydrated through a graded ethanol series and embedded in resin (Low Viscosity Embedding Media Spurr's Kit, EMS, 14300). Ultrathin sections were cut on an ultramicrotome, stained with uranyl acetate and lead citrate, and observed using a JEM-1400 transmission electron microscope (JEOL).

Immunofluorescence

Testes were immediately embedded in OCT compound (Tissue-Tek) and cut into 8 µm sections using a microtome-cryostat (CM1950, Leica). Sections were fixed in 4% PFA for 10 min and then rinsed in PBS three times (pH 7.4), treated with 0.1% Triton X-100 for 10 min and rinsed in PBS three times, blocked in 3% bovine serum albumin (BSA) in PBS for 30 min, and then incubated with primary antibody at 4°C overnight. After three rinses in PBS, the sections were incubated with FITC-conjugated secondary antibody at 1:200 for 1 h at 37°C. DAPI (D3571, Life Technologies) was used to label nuclei. Images were captured immediately using an LSM 780/710 microscope (Zeiss). To examine sperm immunofluorescence, the spermatozoa were washed with PBS three times, plated on coated cover slips, fixed, and then stained as described above.

Immunohistochemistry

Testes were fixed in 4% PFA at 4°C overnight, stored in 70% ethanol, and embedded in paraffin. Sections (5 µm) were deparaffinized and rehydrated, followed by antigen retrieval in 10 mM sodium citrate buffer (pH 6.0) for 15 min. After blocking in 3% BSA and 10% normal goat serum in PBS for 30 min, the sections were incubated with primary antibody at 4°C overnight and then washed in PBS three times. The sections were then treated with 3% H_2O_2 to eliminate internal peroxidase activity. After washing in PBS three times, the sections were stained with HRP-conjugated secondary antibody for 1 h at 37°C. Finally, the sections were stained with 3,3′-diaminobenzidine (DAB) and Haematoxylin. Images were recorded using a Nikon 80i inverted microscope equipped with a CCD camera (Nikon).

Immunoprecipitation and western blotting

Tissue extracts were homogenized in lysis buffer [50 mM Tris-HCl pH 7.4, 420 mM NaCl, 0.1% Triton X-100, 10% glycerol, 0.5% Nonidet P-40, protease inhibitors (Roche), 1 mM PMSF, 1 mM DTT, 10 mM nicotinamide, 10 µM trichostatin A (TSA), 100 µM EX-527 (E7034, Sigma)] using a Dounce homogenizer (1234F35, Thomas Scientific). For immunoprecipitation analysis, the lysates were mixed with antibodies at 4°C overnight, followed by the addition of protein A-Sepharose (GE Healthcare, 17-1279-03). The resulting immunocomplexes were then washed four times with lysis buffer and subjected to western blot analysis.

For the western blot analysis, proteins obtained from lysates or immunoprecipitates were separated by SDS-PAGE and electrotransferred to nitrocellulose membranes. The membranes were then incubated in 5% (w/v) BSA or nonfat milk and stained with the appropriate primary and secondary antibodies. The membrane was scanned using an Odyssey infrared imaging system (Li-Cor Biosciences).

Statistical analysis

All experiments were repeated at least three times and the results are presented as the mean±s.e.m. The distribution of treatment and control groups was analyzed assuming a normal distribution; a homogeneity test of variance showed that their variance was equal. Differences between the treatment and control groups were analyzed using analysis of variance (ANOVA), and differences were calculated using Tukey's test. $P<0.05$ was considered significant.

Acknowledgements

We are grateful to Prof. Wei Liu for providing LC3 constructs and Prof. Qunying Lei for anti-acetyl-lysine antibody.

Competing interests

The authors declare no competing or financial interests.

Author contributions

W.L., F.G., J.J. and Y.G. conceptualized and designed the experiments; C.L., Z.S., L.W., H.Y., Weixiao Liu, Y.S., Z.X., H.Z., Fengyi Gao, J.W. and L.Z. performed the experiments; W.L., C.L. and Z.S. wrote and revised the manuscript. All authors discussed the results and commented on the manuscript.

Funding

This work was supported by the National Natural Science Foundation of China (grants 91519317, 91649202 and 31471277) and National Key R&D Program of China (grant 2016YFA0500901).

Supplementary information

Supplementary information available online at
http://dev.biologists.org/lookup/doi/10.1242/dev.147074.supplemental

References

Abou-Haila, A. and Tulsiani, D. R. P. (2000). Mammalian sperm acrosome: formation, contents, and function. *Arch. Biochem. Biophys.* **379**, 173-182.

Audouard, C. and Christians, E. (2011). Hsp90beta1 knockout targeted to male germline: a mouse model for globozoospermia. *Fertil. Steril.* **95**, 1475-1477 e1471-1474.

Bell, E. L., Nagamori, I., Williams, E. O., Del Rosario, A. M., Bryson, B. D., Watson, N., White, F. M., Sassone-Corsi, P. and Guarente, L. (2014). SirT1 is required in the male germ cell for differentiation and fecundity in mice. *Development* **141**, 3495-3504.

Bingham, N. C., Verma-Kurvari, S., Parada, L. F. and Parker, K. L. (2006). Development of a steroidogenic factor 1/Cre transgenic mouse line. *Genesis* **44**, 419-424.

Boivin, J., Bunting, L., Collins, J. A. and Nygren, K. G. (2007). International estimates of infertility prevalence and treatment-seeking: potential need and demand for infertility medical care. *Hum. Reprod.* **22**, 1506-1512.

Brachmann, C. B., Sherman, J. M., Devine, S. E., Cameron, E. E., Pillus, L. and Boeke, J. D. (1995). The SIR2 gene family, conserved from bacteria to humans, functions in silencing, cell cycle progression, and chromosome stability. *Genes Dev.* **9**, 2888-2902.

Coussens, M., Maresh, J. G., Yanagimachi, R., Maeda, G. and Allsopp, R. (2008). Sirt1 deficiency attenuates spermatogenesis and germ cell function. *PLoS ONE* **3**, e1571.

Cui, Q., Tashiro, S., Onodera, S. and Ikejima, T. (2006). Augmentation of oridonin-induced apoptosis observed with reduced autophagy. *J. Pharmacol. Sci.* **101**, 230-239.

Dam, A. H. D. M., Feenstra, I., Westphal, J. R., Ramos, L., van Golde, R. J. T. and Kremer, J. A. M. (2007). Globozoospermia revisited. *Hum. Reprod. Update* **13**, 63-75.

Dam, A. H., Ramos, L., Dijkman, H. B., Woestenenk, R., Robben, H., van den Hoven, L. and Kremer, J. A. (2011). Morphology of partial globozoospermia. *J. Androl.* **32**, 199-206.

Denu, J. M. (2003). Linking chromatin function with metabolic networks: Sir2 family of NAD(+)-dependent deacetylases. *Trends Biochem. Sci.* **28**, 41-48.

Dobbin, M. M., Madabhushi, R., Pan, L., Chen, Y., Kim, D., Gao, J., Ahanonu, B., Pao, P.-C., Qiu, Y., Zhao, Y. et al. (2013). SIRT1 collaborates with ATM and HDAC1 to maintain genomic stability in neurons. *Nat. Neurosci.* **16**, 1008-1015.

Eskelinen, E.-L., Reggiori, F., Baba, M., Kovács, A. L. and Seglen, P. O. (2011). Seeing is believing: the impact of electron microscopy on autophagy research. *Autophagy* **7**, 935-956.

Fan, W. and Luo, J. (2010). SIRT1 regulates UV-induced DNA repair through deacetylating XPA. *Mol. Cell* **39**, 247-258.

Fujihara, Y., Satouh, Y., Inoue, N., Isotani, A., Ikawa, M. and Okabe, M. (2012). SPACA1-deficient male mice are infertile with abnormally shaped sperm heads reminiscent of globozoospermia. *Development* **139**, 3583-3589.

Gerland, L.-M., Genestier, L., Peyrol, S., Michallet, M.-C., Hayette, S., Urbanowicz, I., Ffrench, P., Magaud, J.-P. and Ffrench, M. (2004). Autolysosomes accumulate during in vitro CD8+ T-lymphocyte aging and may participate in induced death sensitization of senescent cells. *Exp. Gerontol.* **39**, 789-800.

Guarente, L. and Picard, F. (2005). Calorie restriction–the SIR2 connection. *Cell* **120**, 473-482.

Haigis, M. C. and Guarente, L. P. (2006). Mammalian sirtuins–emerging roles in physiology, aging, and calorie restriction. *Genes Dev.* **20**, 2913-2921.

Huang, R., Xu, Y., Wan, W., Shou, X., Qian, J., You, Z., Liu, B., Chang, C., Zhou, T., Lippincott-Schwartz, J. et al. (2015). Deacetylation of nuclear LC3 drives autophagy initiation under starvation. *Mol. Cell* **57**, 456-466.

Jeong, J., Juhn, K., Lee, H., Kim, S.-H., Min, B.-H., Lee, K.-M., Cho, M.-H., Park, G.-H. and Lee, K.-H. (2007). SIRT1 promotes DNA repair activity and deacetylation of Ku70. *Exp. Mol. Med.* **39**, 8-13.

Jimenez, T., Sanchez, G., Wertheimer, E. and Blanco, G. (2010). Activity of the Na,K-ATPase alpha4 isoform is important for membrane potential, intracellular Ca^{2+}, and pH to maintain motility in rat spermatozoa. *Reproduction* **139**, 835-845.

Kang-Decker, N., Mantchev, G. T., Juneja, S. C., McNiven, M. A. and van Deursen, J. M. A. (2001). Lack of acrosome formation in Hrb-deficient mice. *Science* **294**, 1531-1533.

Kierszenbaum, A. L., Rivkin, E. and Tres, L. L. (2003). Acroplaxome, an F-actin-keratin-containing plate, anchors the acrosome to the nucleus during shaping of the spermatid head. *Mol. Biol. Cell* **14**, 4628-4640.

Klionsky, D. J. and Eskelinen, E.-L. (2014). The vacuole versus the lysosome: when size matters. *Autophagy* **10**, 185-187.

Kolthur-Seetharam, U., Teerds, K., de Rooij, D. G., Wendling, O., McBurney, M., Sassone-Corsi, P. and Davidson, I. (2009). The histone deacetylase SIRT1 controls male fertility in mice through regulation of hypothalamic-pituitary gonadotropin signaling. *Biol. Reprod.* **80**, 384-391.

Kullander, S. and Rausing, A. (1975). On round-headed human spermatozoa. *Int. J. Fertil.* **20**, 33-40.

Kume, S., Uzu, T., Horiike, K., Chin-Kanasaki, M., Isshiki, K., Araki, S.-I., Sugimoto, T., Haneda, M., Kashiwagi, A. and Koya, D. (2010). Calorie restriction enhances cell adaptation to hypoxia through Sirt1-dependent mitochondrial autophagy in mouse aged kidney. *J. Clin. Invest.* **120**, 1043-1055.

Lalonde, L., Langlais, J., Antaki, P., Chapdelaine, A., Roberts, K. D. and Bleau, G. (1988). Male infertility associated with round-headed acrosomeless spermatozoa. *Fertil. Steril.* **49**, 316-321.

Lee, I. H., Cao, L., Mostoslavsky, R., Lombard, D. B., Liu, J., Bruns, N. E., Tsokos, M., Alt, F. W. and Finkel, T. (2008). A role for the NAD-dependent deacetylase Sirt1 in the regulation of autophagy. *Proc. Natl. Acad. Sci. USA* **105**, 3374-3379.

Lee, S.-Y., Lee, H., Kim, E.-S., Park, S., Lee, J. and Ahn, B. (2015). WRN translocation from nucleolus to nucleoplasm is regulated by SIRT1 and required for DNA repair and the development of chemoresistance. *Mutat. Res.* **774**, 40-48.

Lin, Y.-N., Roy, A., Yan, W., Burns, K. H. and Matzuk, M. M. (2007). Loss of zona pellucida binding proteins in the acrosomal matrix disrupts acrosome biogenesis and sperm morphogenesis. *Mol. Cell. Biol.* **27**, 6794-6805.

Lin, Y.-H., Yuan, J., Pei, H., Liu, T., Ann, D. K. and Lou, Z. (2015). KAP1 deacetylation by SIRT1 promotes non-homologous end-joining repair. *PLoS ONE* **10**, e0123935.

Lomeli, H., Ramos-Mejia, V., Gertsenstein, M., Lobe, C. G. and Nagy, A. (2000). Targeted insertion of Cre recombinase into the TNAP gene: excision in primordial germ cells. *Genesis* **26**, 116-117.

Martinez-Redondo, P. and Vaquero, A. (2013). The diversity of histone versus nonhistone sirtuin substrates. *Genes Cancer* **4**, 148-163.

Mason-Garcia, M., Vigh, S., Comaru-Schally, A. M., Redding, T. W., Somogyvari-Vigh, A., Horvath, J. and Schally, A. V. (1985). Radioimmunoassay for 6-D-tryptophan analog of luteinizing hormone-releasing hormone: measurement of serum levels after administration of long-acting microcapsule formulations. *Proc. Natl. Acad. Sci. USA* **82**, 1547-1551.

McBurney, M. W., Yang, X., Jardine, K., Hixon, M., Boekelheide, K., Webb, J. R., Lansdorp, P. M. and Lemieux, M. (2003). The mammalian SIR2alpha protein has a role in embryogenesis and gametogenesis. *Mol. Cell. Biol.* **23**, 38-54.

Meuwissen, R. L., Offenberg, H. H., Dietrich, A. J., Riesewijk, A., van Iersel, M. and Heyting, C. (1992). A coiled-coil related protein specific for synapsed regions of meiotic prophase chromosomes. *EMBO J.* **11**, 5091-5100.

Ng, F. and Tang, B. L. (2013). Sirtuins' modulation of autophagy. *J. Cell. Physiol.* **228**, 2262-2270.

Paiardi, C., Pasini, M. E., Gioria, M. and Berruti, G. (2011). Failure of acrosome formation and globozoospermia in the wobbler mouse, a Vps54 spontaneous recessive mutant. *Spermatogenesis* **1**, 52-62.

Payne, A. H., Downing, J. R. and Wong, K.-L. (1980). Luteinizing hormone receptors and testosterone synthesis in two distinct populations of leydig cells. *Endocrinology* **106**, 1424-1429.

Pierre, V., Martinez, G., Coutton, C., Delaroche, J., Yassine, S., Novella, C., Pernet-Gallay, K., Hennebicq, S., Ray, P. F. and Arnoult, C. (2012). Absence of Dpy19l2, a new inner nuclear membrane protein, causes globozoospermia in mice by preventing the anchoring of the acrosome to the nucleus. *Development* **139**, 2955-2965.

Saunders, L. R. and Verdin, E. (2007). Sirtuins: critical regulators at the crossroads between cancer and aging. *Oncogene* **26**, 5489-5504.

Singh, G. (1992). Ultrastructural features of round-headed human spermatozoa. *Int. J. Fertil.* **37**, 99-102.

Smith, J. S., Brachmann, C. B., Celic, I., Kenna, M. A., Muhammad, S., Starai, V. J., Avalos, J. L., Escalante-Semerena, J. C., Grubmeyer, C., Wolberger, C. et al. (2000). A phylogenetically conserved NAD^+-dependent protein deacetylase activity in the Sir2 protein family. *Proc. Natl. Acad. Sci. USA* **97**, 6658-6663.

Svechnikova, K., Svechnikova, I. and Söder, O. (2011). Gender-specific adverse effects of mono-ethylhexyl phthalate on steroidogenesis in immature granulosa cells and rat leydig cell progenitors in vitro. *Front. Endocrinol.* **2**, 9.

Venables, J. P. and Cooke, H. J. (2000). Lessons from knockout and transgenic mice for infertility in men. *J. Endocrinol. Invest.* **23**, 584-591.

Wang, R.-H., Sengupta, K., Li, C., Kim, H.-S., Cao, L., Xiao, C., Kim, S., Xu, X., Zheng, Y., Chilton, B. et al. (2008). Impaired DNA damage response, genome instability, and tumorigenesis in SIRT1 mutant mice. *Cancer Cell* **14**, 312-323.

Wang, H. N., Wan, H. F., Li, X. X., Liu, W. X., Chen, Q., Wang, Y. Q., Yang, L., Tang, H. M., Zhang, X. J., Duan, E. K. et al. (2014). Atg7 is required for acrosome biogenesis during spermatogenesis in mice. *Cell Res.* **24**, 852-869.

Xiao, N., Kam, C., Shen, C., Jin, W., Wang, J., Lee, K. M., Jiang, L. and Xia, J. (2009). PICK1 deficiency causes male infertility in mice by disrupting acrosome formation. *J. Clin. Invest.* **119**, 802-812.

Xu, X., Toselli, P. A., Russell, L. D. and Seldin, D. C. (1999). Globozoospermia in mice lacking the casein kinase II alpha' catalytic subunit. *Nat. Genet.* **23**, 118-121.

Yao, R., Ito, C., Natsume, Y., Sugitani, Y., Yamanaka, H., Kuretake, S., Yanagida, K., Sato, A., Toshimori, K. and Noda, T. (2002). Lack of acrosome formation in mice lacking a Golgi protein, GOPC. *Proc. Natl. Acad. Sci. USA* **99**, 11211-11216.

Yildiz, Y., Matern, H., Thompson, B., Allegood, J. C., Warren, R. L., Ramirez, D. M. O., Hammer, R. E., Hamra, F. K., Matern, S. and Russell, D. W. (2006). Mutation of beta-glucosidase 2 causes glycolipid storage disease and impaired male fertility. *J. Clin. Invest.* **116**, 2985-2994.

Yuan, Z., Zhang, X., Sengupta, N., Lane, W. S. and Seto, E. (2007). SIRT1 regulates the function of the Nijmegen breakage syndrome protein. *Mol. Cell* **27**, 149-162.

Zeng, R., He, J., Peng, J., Chen, Y., Yi, S., Zhao, F. and Cui, G. (2012). The time-dependent autophagy protects against apoptosis with possible involvement of Sirt1 protein in multiple myeloma under nutrient depletion. *Ann. Hematol.* **91**, 407-417.